

12-14-2015

# Optical Second Harmonic Generation in the BaTiO<sub>3</sub> Phase on Magnetically Aligned Multiferroic Nanofibers

Katia Gasperi

*University of South Carolina - Columbia*

Follow this and additional works at: <http://scholarcommons.sc.edu/etd>

 Part of the [Physics Commons](#)

---

## Recommended Citation

Gasperi, K.(2015). *Optical Second Harmonic Generation in the BaTiO<sub>3</sub> Phase on Magnetically Aligned Multiferroic Nanofibers*. (Master's thesis). Retrieved from <http://scholarcommons.sc.edu/etd/3271>

This Open Access Thesis is brought to you for free and open access by Scholar Commons. It has been accepted for inclusion in Theses and Dissertations by an authorized administrator of Scholar Commons. For more information, please contact [SCHOLARC@mailbox.sc.edu](mailto:SCHOLARC@mailbox.sc.edu).

# Optical Second Harmonic Generation in the BaTiO<sub>3</sub> phase of magnetically aligned multiferroic nanofibers

by

Katia Gasperi

Master of Nanophysics, Nanocomponents, and Nano-measurements  
Paul Sabatier University / National Institute of Applied Sciences, 2003

---

Submitted in Partial Fulfillment of the Requirements

For the Degree of Master of Science in

Physics

College of Arts and Sciences

University of South Carolina

2015

Accepted by:

Yanwen Wu, Director of Thesis

Thomas Crawford, Reader

Lacy Ford, Senior Vice Provost and Dean of Graduate Studies

## **Acknowledgements**

I want to thank my advisor Dr. Wu for her guidance and for sharing her immense knowledge; thanks to Dr. Crawford and his team for promoting collaboration and sharing their sample and equipment; thanks to Dr. Crittenden for sharing his knowledge and equipment; thanks to Dr. Webb for his patience, availability, experience and equipment; thanks to all of Dr. Wu's team; thanks to Fiona Oxsher for sharing her knowledge concerning the photolithography projector; thanks to Arthur Illingworth and Allen Frye for all their detailed and crucial advice concerning the milling machine; thanks to James Clawson for his constant availability as well as for the oscilloscope, the wires, the power supply, the crimping tools, the connectors, the variable, the computer,...etc..; and thanks to Zachary Marsh, and Warren Steckle, for letting me use the SAXS Lab.

I also want to thank all the professors whose courses contributed to this work, especially Dr. Bazaliy for his magnetism class, Dr. Creswick for his solid state physics class, and Dr. Kunchur for his topics class; I want to thank all the "librarian chatters" for finding important articles at any time of the day; thanks to Beth Powell, Lisa Saxon, Evelyn Wong, Amanda Davis, Kelly Gibson, Sam Beals for their hard work and their kindness; thanks to the maintenance team for all their help; thanks to the cleaning team for their work and their everyday smile; thanks to Nahid Shayesteh Moghadam, Barnali Chowduri, Lei Wang,

Leila Aneta Net for their support and encouragement, and special thanks to David Edelson for improving every single day my English, step by step.

Finally I want to thank all my friends and family among the greats who gave me the strength of achieving this work: Sarah Gasperi, Danielle Gasperi, Rebecca Gasperi, Jacques Gasperi, Bernard Maruejous, Daniel Beau, Solange Mottal, Jacques Mottal, Christine Morrison, Peter Morrison, Mary Bull, Craig Kridel, Fabrice Gil, Fabrice Benhamou, Pascale Marty, Marianne Cathalat, Ocine Himeur, Frederique Faure, E Richard Walton, Akelina cherie, Veronique Correch, Olivier Danger, Sandrine Dupuy, Jacqueline Masnari, Carole Chalut, Claudine Urquhart, Regine Dufaur, Michel Dufaur, Julie Hubbert, Laetitia Pont, Sandrine Buhours, Nelly Garzon, Desiré Nguessan, Hinda Boudiaf, Stefanie Mellet, Theodore Monod, Yasmina Khadra, Coluche, Guillaume Galliene, l'Abbé Pierre, Albert Camus, Jacques Prevert, and Antoine de Saint-Exupery.

## **Abstract**

Multiferroic materials enable the exploration of electrical control of magnetic properties and vice versa. Their increasing interest is especially due to their potential applications in the industry of information storage. Thanks to recent progress in nanotechnology, they have also been found to have many other applications such as transducers and sensors, and they already occupy a unique place in the biomedical field. The objective of this project is to study multiferroic nanofibers made of cobalt ferrite  $\text{CoFe}_2\text{O}_4$  (CFO) and barium titanate  $\text{BaTiO}_3$  (BTO) with a specific focus in the characterization of the ferroelectric phase. We researched the state of knowledge concerning the size effects on phase transition for nanoparticles and polycrystals BTO. The ferroelectric phase transition of BTO occurs when it changes from a tetragonal (anisotropic) crystal structure to a cubic (isotropic) structure. This change suggests that optical second harmonic generation (SHG) is a good measurement technique for monitoring the phase transition of the BTO half of the nanofibers. We designed and prepared a temperature dependent SHG experiment on magnetically aligned fibers in transmission with the possibility to investigate the polarization dependence of the signal. We also prepared interdigital electrodes on glass for the future study of the fibers in an external electric field.

## Table of Contents

<b>Acknowledgements .....</b>	<b>ii</b>
<b>Abstract.....</b>	<b>iv</b>
<b>List of tables .....</b>	<b>vii</b>
<b>List of figures .....</b>	<b>viii</b>
<b>Chapter 1: Motivations for the study of multiferroic materials. ....</b>	<b>1</b>
<b>Chapter 2: Preliminary studies: barium titanate BaTiO<sub>3</sub> .....</b>	<b>6</b>
1. Perovskites:.....	6
2. Bulk material: different crystals, ferroelectricity, T dependance .....	7
3. Size effect.....	9
4. Optical Second Harmonic Generation (SHG) .....	12
<b>Chapter 3: Experimental section.....</b>	<b>18</b>
1. Experimental design and expectations.....	18
2. Sample preparation .....	19
3. Sample holder and sample mount.....	23
4. Experiment alignment for SHG in transmission.....	26
5. Interdigital electrodes on glass.....	28

6. Future plans: conduct of the experiment .....	31
<b>Glossary.....</b>	<b>33</b>
<b>References.....</b>	<b>36</b>

## List of tables

Table 1.1 Electric and magnetic properties .....	4
Table 2.1 Optical SHG coefficients for bulk barium titanate .....	16
Table 2.2 Optical SHG coefficients for BaTiO <sub>3</sub> on MgO[14] .....	17
Table 3.1 Calibration: mount used with one heater alone.....	25
Table 3.2 Calibration: mount used with the two heaters together (A and B) .....	26



## List of figures

Figure 1.1 Relationship between multiferroic and magnetoelectric materials[1].	2
Figure 2.1 Structure of a perovskite with a chemical formula $ABX_3$	6
Figure 2.2 Phase transitions for barium titanate[6]	7
Figure 2.3 Cubic Tetragonal phase transition @ DoITPoMS, University of Cambridge	8
Figure 2.4 Ti movement in the O octahedra @ DoITPoMS, University of Cambridge	9
Figure 2.5 Change in tetragonality $c/a$ with particle size at room temperature[10]	10
Figure 2.6 DSC measurements for $BaTiO_3$ polycrystals with different grain sizes[11]	11
Figure 3.1 Sample I prepared by the Dr. Crawford's Team on glass	20
Figure 3.2 Sample II prepared by Dr. Crawford's Team on glass	20
Figure 3.3 Fibers in interdigital electrodes	21
Figure 3.4 Sample on glass (aligned under 2.36kG after vortex agitation)	21
Figure 3.5 Sample on mica	22
Figure 3.6 Sample holder	23
Figure 3.7 Heaters A and B	24
Figure 3.8 Heater A configuration (back side)	24
Figure 3.9 Heater B configuration (front side)	24
Figure 3.10 A + B configuration	25
Figure 3.11 Experiment design	27

Figure 3.12 Measurements made for a line width of 20 points .....	29
Figure 3.13 Measurements made for a line width of 50 points .....	29
Figure 3.14 Measurements made for a line width of 100 points .....	30
Figure 3.15 Calibration for the projection photolithography .....	30
Figure 3.16 Sample holder .....	31
Figure 3.17 Interdigital electrodes.....	31

## **Chapter 1: Motivations for the study of multiferroic materials.**

This work is part of a project involving multiferroic nanofibers made of cobalt ferrite  $\text{CoFe}_2\text{O}_4$  (CFO) and barium titanate  $\text{BaTiO}_3$  (BTO) in collaboration between Dr. Crawford's group and Dr. Wu's group. Its ultimate goal is to study the coupling between the two phases. The context and motivations to study this CFO/BTO multiferroic material will be discussed in this chapter. The investigation will then concentrate on the ferroelectric phase characterization of barium titanate, which is the main objective of this specific work. Details of this investigation will be discussed in the second and third chapter.

The increasing interest concerning multiferroic and magnetoelectric materials is especially due to their potentially long-term applications in the industry of information storage[1]. In addition, being a part of the "smart materials," they find a multitude of applications such as transducers or magnetic field sensors[2] as well as occupy a unique place in the field of biomedical[3]. While multiferroic and magnetoelectric materials can be single phase, most of them are multiphase. The meaning of "multiferroic" has evolved since such materials have been studied, and its current definition is a material that possesses two or more ferroic properties (cf. fig. 1.1).

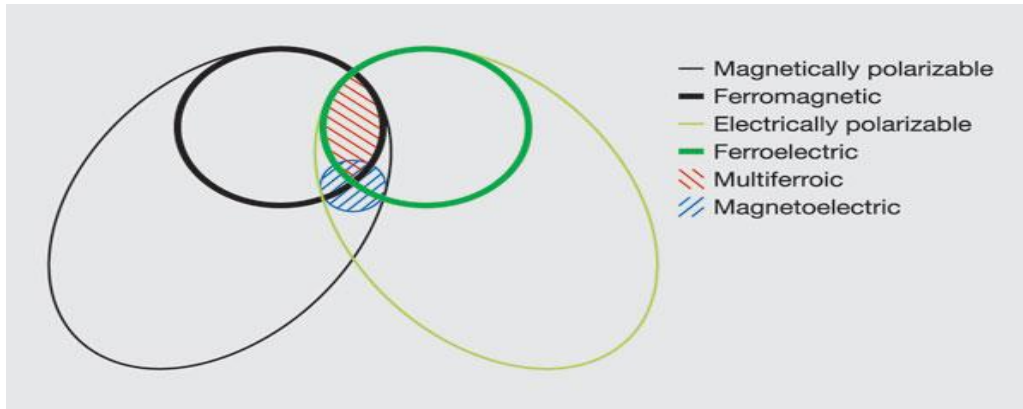


Figure 1.1 Relationship between multiferroic and magnetoelectric materials[1].

For the information storage application, magnetoelectric coupling is the key: It allows for the writing of data electrically (avoiding the necessity to generate a high field to write magnetically) and for the reading of data magnetically (avoiding the problems to electrically read ferroelectric random access memory FeRAMs, which is usually a destructive process). The magnetoelectric coupling may arise from any magnetic and electric order. This coupling could happen directly between the two orders or indirectly, for example via strain. For a multiphase multiferroic system, the strain due to the interface of the two materials often plays an important role. Indirect coupling via strain could result in interesting properties such as piezomagnetism, magnetostriction, piezoelectric, electrostriction (see glossary for detailed definitions). First, we consider the magnetoelectric coupling without any mechanical stress or strain involved. The free energy determines the behavior of the material and its response to a magnetic or electric field.

Using the Einstein summation convention, the free energy of a system in response to an electric field  $E$  and a magnetic field  $H$  could be expressed as:

$$-F(E, H) = \frac{1}{2} \epsilon_0 \epsilon_{ij} E_i E_j + \frac{1}{2} \mu_0 \mu_{ij} H_i H_j + \alpha_{ij} E_i H_j + \frac{1}{2} \beta_{ijk} E_i H_j H_k + \frac{1}{2} \gamma_{ijk} H_i E_j E_k$$

where,

- $\epsilon_{ij}$  (relative permittivity tensor) is temperature dependent,
- $\mu_{ij}$  (relative permeability tensor) is temperature dependent,
- $\alpha_{ij}$  is a linear magnetoelectric coupling coefficient and is temperature dependent,
- $\beta_{ijk}$  and  $\gamma_{ijk}$  are quadratic magnetoelectric coupling coefficients and are temperature dependent.

Note that we have ignored higher coupling orders in this expression. However, it is important to keep in mind that couplings involving higher rank tensor than  $\alpha_{ij}$  might become dominant in many cases. As an example,  $\beta_{ijk} H_j H_k$  dominates  $\alpha_{ij} H_j$  in the piezoelectric paramagnet  $\text{NiSO}_4 \cdot 6\text{H}_2\text{O}$  [4]. In general, the coupling coefficients are rather difficult to determine and highly dependent on the structure of the materials. Now, if we want to include the couplings via mechanical stress or strain, cross terms need to be added in the free energy equation above. The coupling will become even more difficult to characterize.

In order to catch a glimpse of all the possible combinations among multiferroics, the following table gives a list of properties between which couplings may occur (see glossary for the corresponding definitions of the properties):

Table 1.1 Electric and magnetic properties

<b>Electric properties</b>	<b>Magnetic properties</b>
Ferroelectric	Ferromagnetic
Ferrielectric	Ferrimagnetic
Antiferroelectric	Antiferromagnetic
Piezoelectric	Piezomagnetic
Electrostriction	Magnetostriction
Flexoelectric	
Ferrotoroidic	

Among these properties, ferroelectric and ferrimagnetic are expected to be the dominant ones in our cobalt ferrite / barium titanate (CFO/BTO) nanofibers sample. The CFO part is ferrimagnetic and the BTO part is ferroelectric. The fiber as a whole is multiphase where strain is expected to be the main coupling mechanism. However, before we can achieve and analyze coupling between the two phases, we need to fully understand the two phases separately. In this project, we will investigate the ferroelectric BTO phase. The plan of the experiment builds on the state of knowledge in the field, more specifically on the size effects affecting phase transitions, ferroelectricity and optical properties of barium titanate nanoparticles (NPs) and polycrystals (PCs): this will be discussed in the

second chapter. We will discuss how the crystal symmetry changes from isotropic to anisotropic during the cubic-tetragonal phase transition. This structural change means that the optical second harmonic generation (SHG) is a good measurement tool for monitoring the corresponding phase transition. As a result, an optical SHG experiment have been prepared and its setup will be described in the third chapter.

## Chapter 2: Preliminary studies: barium titanate BaTiO<sub>3</sub>

### 1. Perovskites:

Barium titanate is part of the perovskite family. Perovskites structures ( $X^{II}A^{2+}VI B^{4+}X^{2-}_3$ ) have been studied theoretically as well as experimentally, and they occupy a quite important class in material science. Each individual compound of this family has its own interest. The structure of highest symmetry is cubic (fig. 2.1, retrieved from Wikipedia common).

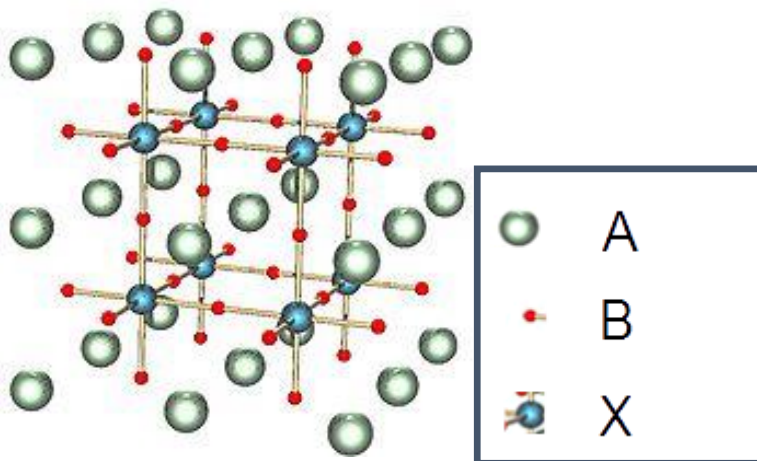


Figure 2.1 Structure of a perovskite with a chemical formula ABX<sub>3</sub>



There are, however, many types of distortion that could occur in the bulk structure of this family, such as:

- distortion of the whole structure (for example, elongation in a particular direction),
- A displacement,
- B displacement,
- octahedron rotation,
- octahedron distortion.

During the past 15 years, progress in nanotechnology and computation resulted in new avenues of research for this material and, more recently, have revealed some interesting mechanisms such as “oxygen breathing motion” resulting in magnetic properties for this material[5]. For the purpose of this work, we will focus on barium titanate  $\text{BaTiO}_3$  as a bulk material in the range tetragonal - cubic and will concentrate on ferroelectric and non-linear optical properties.

## 2. Bulk material: different crystals, ferroelectricity, T dependance

The bulk material exists in five phases, with the following transition temperatures:

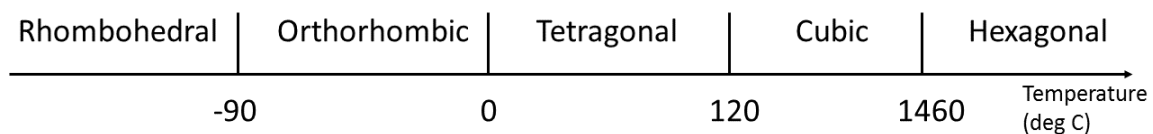


Figure 2.2 Phase transitions for barium titanate[6]

The cubic phase is paraelectric and the tetragonal is ferroelectric. The corresponding transition is a first order phase transition (in agreement with latent heat measurements and simulations[7]) but is close to a second order phase transition. Studies revealed a mixed behavior displacive and order disorder (see glossary for detailed definitions)[7][8][9]. Simulation of the phase transitions using an effective Hamiltonian, including low energy distortions only, have demonstrated a good agreement with experiments on bulk materials [7]. The ferroelectricity appears with the tetragonality, below 120°C. During the phase transition between cubic and tetragonal, the atom displacements allow the production of a dipole moment (fig. 2.3).

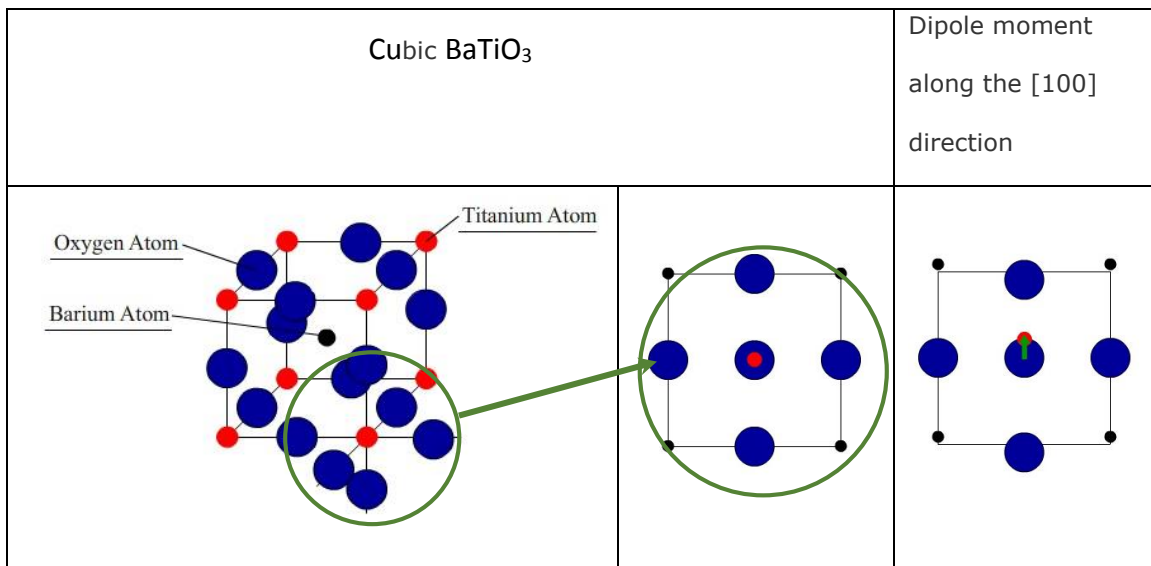


Figure 2.3 Cubic-tetragonal phase transition © DoITPoMS, University of Cambridge

It is important to note that the next orthorhombic and rhombohedral phases are ferroelectric as well. These phases differ from the cubic phase by a displacement of the titanium atom in the oxygen octahedron, along different directions (cf. fig. 2.4).

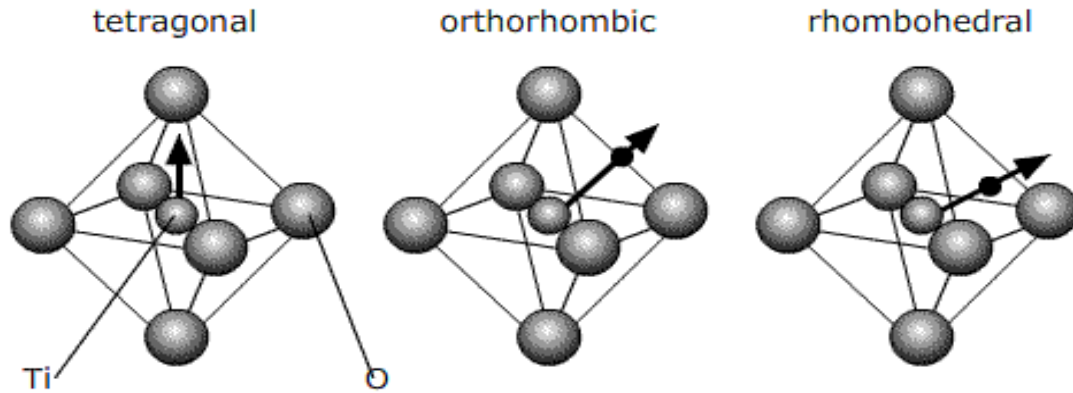


Figure 2.4 Ti movement in the O octahedra © DoITPoMS, University of Cambridge

### 3. Size effect

The structural and physical properties of  $\text{BaTiO}_3$  are dramatically size-dependent, even for fine ceramics with grain size as large as  $1 \mu\text{m}$ . Different studies have already been conducted to determine how the size and shape of  $\text{BaTiO}_3$  could affect the phase transition temperatures, the ratio of the lattice parameters  $c/a$  at a fixed temperature, the ferroelectric properties, and even optical SHG. Even though the results also depend on the various techniques used to prepare the material itself, they have a common trend. They had been carefully analyzed and documented by Jian Yu and Junhao Chu for the ENN (Encyclopedia of Nanoscience and Nanotechnology)[8].

a. Influence on the phase transition tetragonal - cubic temperature

The tetragonal-cubic phase transition temperature decreases significantly for small particles. At room temperature, the tetragonality is affected for particle sizes ranging from 120 nm to 300 nm. Results from X-ray diffraction (XRD), transmission electron microscopy (TEM) and specific surface area measurements on barium titanate powders lead to a “critical size” of the cubic-tetragonal transition of about 120 nm (fig. 2.5).

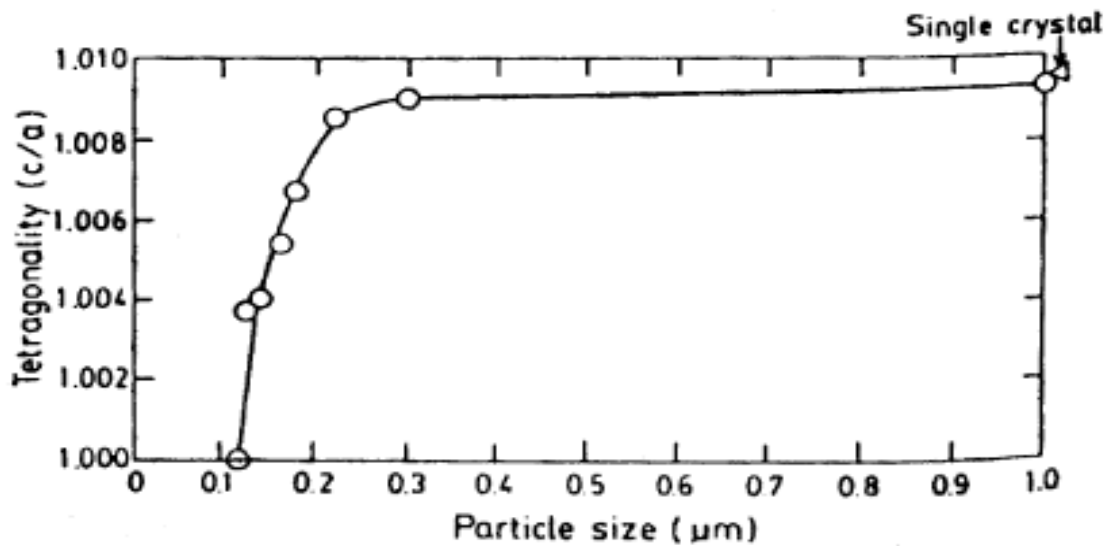


Figure 2.5 Change in tetragonality  $c/a$  with particle size at room temperature[10]

The critical size of the tetragonal cubic transition at room temperature for NPs was found to be between 50 nm and 90 nm depending on different synthesis methods and different measurement techniques[11][10][12][13]. Differential scanning calorimetry (DSC) measurements had also been performed on polycrystals: the cubic-tetragonal phase transition shifts to a slightly lower temperature, and the orthorhombic shifts to a slightly

higher temperature. But below 100nm, DSC measurements do not reveal the phase transition temperatures anymore (fig. 2.6).

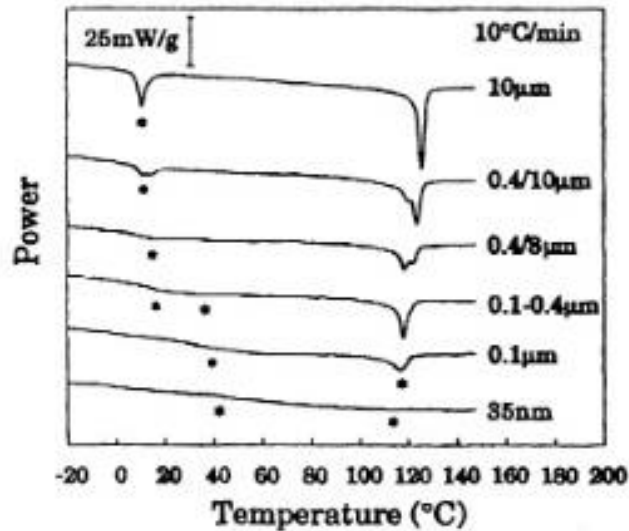


Figure 2.6 DSC measurements for BaTiO<sub>3</sub> polycrystals with different grain sizes[11]

To conclude this short analysis concerning size effects on phase transitions, we can say that the discrepancies about the temperature of the cubic-tetragonal phase transition depend on the synthesis techniques of NPs, the measurement methods (XRD, TEM, scanning electron microscopy SEM, DSC), but also the strain or boundaries associated with the type of material. For example, the strain induced by MgO on thin film increases the tetragonality[14], but XRD measurements trend to prove that the core of nanocrystals remains tetragonal while the surface relaxes to a cubic phase[15]: strain, surface effects become predominant below 100nm.

#### b. Influence on the dielectric constant temperature dependence

Due to the size dependence of the cubic-tetragonal phase transition, the ferroelectric phase transition temperature  $T_c$  decreases with decreasing grain size similarly to the cubic-tetragonal phase transition [10]. Below 1  $\mu\text{m}$ , however, the permittivity decreases with decreasing size. The P-E hysteresis cycle is still present for NPs ranging between 1.2  $\mu\text{m}$  and 0.3  $\mu\text{m}$ , but the coercive field may vary (in the range of 0.22 MV/m to 0.11 MV/m); the remanent and spontaneous polarizations both decrease with the size [16]. Again, those results could vary with synthesis techniques and/or presence of defects, but they emphasize the predominance of surface effects as well as the possible presence of different phases. Also, below 1  $\mu\text{m}$ , there is a loss of long range cooperative interaction and twins effect, which usually participate in the domain formations for the bulk material [11][17]. To conclude, XRD measurements even combined with TEM, SEM, DSC, cannot give alone a deep understanding of the structure changes in barium titanate at low scale, which conducted the scientific community to perform optics experiments.

#### 4. Optical Second Harmonic Generation (SHG)

A good understanding of optical SHG should require a quantum mechanics description especially for a nanomaterial; however, a classical approach gives a quite reliable description for the bulk material.

a. Optical SHG for the bulk crystal: classical description[18]

Optical SHG requires some nonlinear dielectric properties: the polarization  $P$  of a crystal due to an external field  $E$  should have a component proportional to the square of the field.

The polarization in a crystal comes from the displacement of electrons in an electric field:

$$p(t) = -nex(t)$$

In this equation,  $n$  is the electronic density,  $e$  the charge of electron, and  $x(t)$  is the electrons displacement from their equilibrium position.

- For a symmetric potential  $V(x)$ , (cf. one direction of the cubic case):

$$V(x) = V(-x) = \frac{1}{2} m \omega_0^2 x^2 + o(x^3)$$

where  $m$  is the electron mass and  $\omega_0$  is the resonance frequency of the electronic oscillator.

The corresponding restoring force is:

$$F = -m \omega_0^2 x + o(x^2)$$

For a field  $E^{(\omega)}(t)$ , with  $\omega$  small compare to  $\omega_0$ ,

$$F = -eE(t) \quad \Rightarrow \quad x(t) = -\frac{e}{m \omega_0^2} E(t)$$

In this case, the polarization is directly proportional to the field: the signal generated by light interaction with a p-wave does not depend on the light polarization.

- For an asymmetric potential  $V(x)$ , (cf. one direction of the tetragonal case), the potential can be approximated as:

$$V(x) = \frac{1}{2} m \omega_0^2 x^2 + \frac{1}{3} m D x^3 + o(x^3)$$

The corresponding restoring force is:

$$F = -m \omega_0^2 x + m D x^2 + o(x^2)$$

In this case, for a driven field  $E^{(\omega)}(t) = E^{(\omega)} \cos \omega t$ , with  $\omega$  small compare to  $\omega_0$ , taking into account the possible losses (absorption),  $x(t)$  is solution of the following equation:

$$\frac{d^2 x}{dt^2} + \sigma \frac{dx}{dt} + \omega_0^2 x + D x^2 = -\frac{eE^{(\omega)}}{2m} (e^{i\omega t} + e^{-i\omega t})$$

The solution is  $x(t) = \frac{1}{2}(q_1 e^{i\omega t} + q_2 e^{2i\omega t} + q_1^* e^{-i\omega t} + q_2^* e^{-2i\omega t})$

with  $q_1 = -\frac{eE^{(\omega)}}{2m} \frac{1}{(\omega_0^2 - \omega^2) + i\omega\sigma}$  and  $q_2 = \frac{-De^2[E^{(\omega)}]^2}{2m^2[(\omega_0^2 - \omega^2) + i\omega\sigma]^2[\omega_0^2 - 4\omega^2 + 2i\omega\sigma]}$

The resulting polarizations are:

$$p^{(\omega)}(t) = -\frac{ne}{2} (q_1 e^{i\omega t} + q_1^* e^{-i\omega t}) \quad \text{and} \quad p^{(2\omega)}(t) = -\frac{ne}{2} (q_2 e^{2i\omega t} + q_2^* e^{-2i\omega t})$$

It is normal to define the nonlinear optical coefficients  $d$  as:

$$p^{(2\omega)}(t) = -\frac{1}{2} (d^{(2\omega)} q_2 [E^{(\omega)}]^2 e^{2i\omega t} + c. c.)$$



Using the full expression for  $q_2$ , we get:

$$d^{(2\omega)} = \frac{-Dne^3}{2m^2[(\omega_0^2 - \omega^2) + i\omega\sigma]^2[\omega_0^2 - 4\omega^2 + 2i\omega\sigma]}$$

This coefficient can also be rewritten in term of the susceptibility as:

$$d^{(2\omega)} = \frac{mD[\chi^{(\omega)}]^2\chi^{(2\omega)}\epsilon_0^3}{2n^2e^3}$$

A simple expression for the resulting amplitude polarization can be obtained:

$$P^{(2\omega)} = d^{(2\omega)}E^{(\omega)}E^{(\omega)}$$

These last expressions have given good predictions of the polarization for different ferroelectric materials.[19]

In three dimensions,

$$P_i^{(2\omega)} = d_{ijk}^{(2\omega)} E_j^{(\omega)} E_k^{(\omega)}$$

A good estimate of the nonlinear optical coefficients  $d_{ijk}^{(2\omega)}$  can be found from this calculation for barium titanate.

#### b. Known nonlinear optical coefficients for BaTiO<sub>3</sub>

Since the development of this classical concept, different measurement techniques for the  $d_{ijk}^{(2\omega)}$  have emerged[20]. From those measurements, the coefficients are usually

given in pm/V for a specific incident wavelength and are well known for the bulk BaTiO<sub>3</sub> (cf. table 2.1) [14].

Table 2.1 Optical SHG coefficients for bulk barium titanate

	Optical SHG coefficient (pm/V) at 1.064μm
$d_{15} \equiv d_{113}$	17.0
$d_{33} \equiv d_{333}$	6.8
$d_{31} \equiv d_{311}$	15.7

c. Size effects:

As the size decreases, the orbital hybridizations and the tetragonal distortions decrease, leading to smaller optical SHG coefficients. The SHG signal becomes weaker but can still be measured and may eventually be used to determine the phase transition temperature or the critical size. Some experiments had already been conducted:

- The SHG signal from small grains of about 35nm is 10<sup>3</sup> weaker than the ones generated by grains of about 10 μm[11].
- The SHG signal from barium titanate thin film grown by metal organic chemical vapor deposition (MOCVD) on magnesium oxide gives lower values for the optical coefficients, even though the deposition technique and the strain involved are assumed to increase the tetragonality in BaTiO<sub>3</sub> (table 2.2).

Table 2.2 Optical SHG coefficients for BaTiO<sub>3</sub> on MgO[14]

	d (pm/V) at 1.064 $\mu\text{m}$
c oriented film	2.13
a oriented film	1.5

- SHG measurements with incoming signal polarization dependence reveal the presence of tetragonality in BaTiO<sub>3</sub> NPs with size ranging between 22nm and 55nm. Also, the direction of the a and c axis can be deduced from the measurements[21].

## Chapter 3: Experimental section

### 1. Experimental design and expectations

Following the previous study, an optical SHG experiment to characterize the multiferroic nanofibers CFO/BTO had been prepared, with capabilities of:

- temperature dependence,
- excitation light polarization dependence,
- possibilities to investigate the response of the multiferroic nanofibers to an external electric field.

The main objective of the experiment is to observe the temperature dependence of the signal to monitor the Curie temperature. The ferromagnetic phase of the fibers has been used to magnetically align the fibers. Variations of SHG signal intensity with respect to the temperature are expected to detect the Curie temperature, while changes of SHG signal intensity versus incoming light polarization can confirm the presence of the tetragonal phase and give the angle between the a and c axis of the ferroelectric phase. The magnetic alignment gives the possibility to select one single fiber or a group of fibers close to each other, aligned in the same direction.

Further work with the addition of an external electric field are planned: different interdigital electrodes on glass had been prepared for that purpose. The magnetic alignment of the fibers allows for the selection of an external electric field's particular direction with respect to the axis of the fibers. With this new ingredient, a change in intensity of the SHG signal versus the polarization of light with the addition of the external electric field may emphasize any privileged direction for the polarization dependent SHG signal with respect to the fiber axis.

## 2. Sample preparation

The nanofibers were aligned on a transparent substrate in a magnetic field of about 2.36kG via the ferrimagnetic CFO phase (at room temperature). Two substrates were used: mica, for X-ray diffraction measurement, and glass, for the transmission experiment. The fibers seem to agglomerate differently depending on:

- the agitation of the solution before deposition,
- the time spent between the agitation and the deposition,
- the wetting between the solution and the substrate,
- the eventual contamination of the solution.

Different samples have been prepared for this project (cf. fig. 3.1, 3.2, 3.3, 3.4 and 3.5).

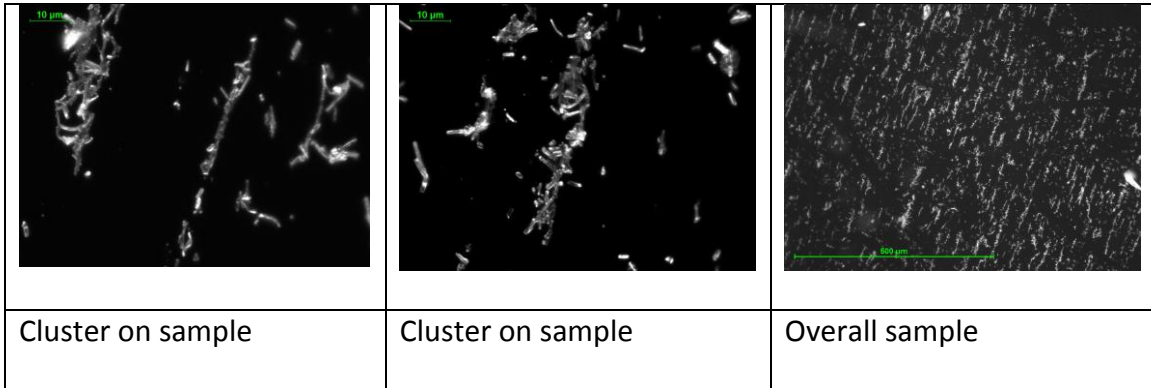


Figure 3.1 Sample I prepared by the Dr. Crawford's Team on glass

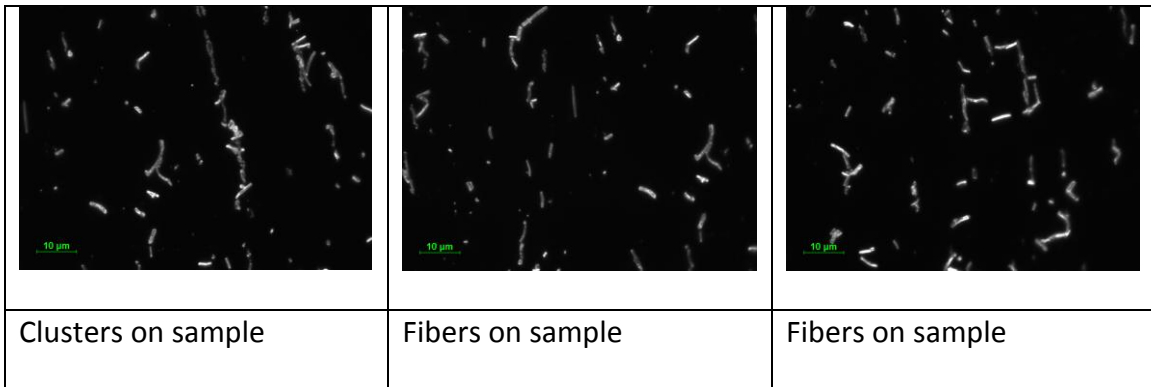


Figure 3.2 Sample II prepared by Dr. Crawford's Team on glass

It can be seen from the figures 3.1 and 3.2 that the alignment is well realized when the fibers are far enough, but they could form clusters made of fibers with different directions due to the magnetization of the ferrimagnetic phase.

Some fibers have successfully been aligned in a direction parallel to interdigital electrodes, allowing an experiment with an external electric field perpendicular to the axis of the fibers (fig. 3.3). Additional samples have been prepared on glass (fig. 3.4) and mica (fig. 3.5).

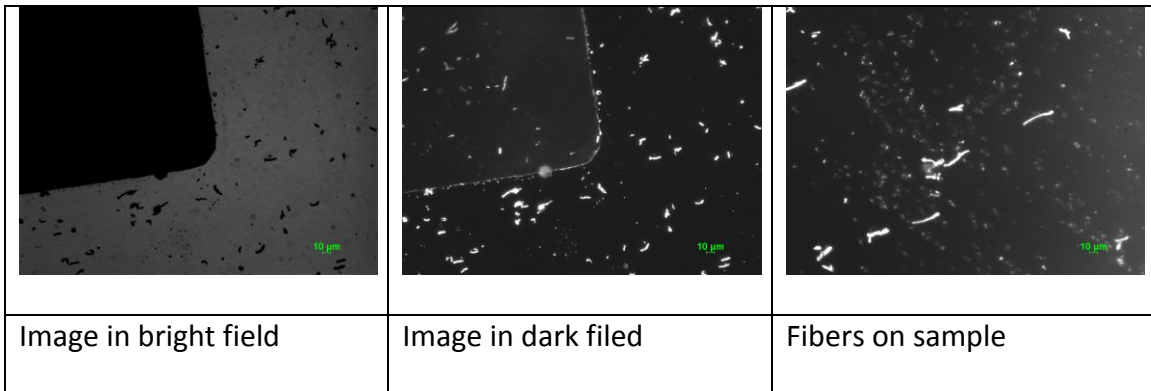


Figure 3.3 Fibers in interdigital electrodes

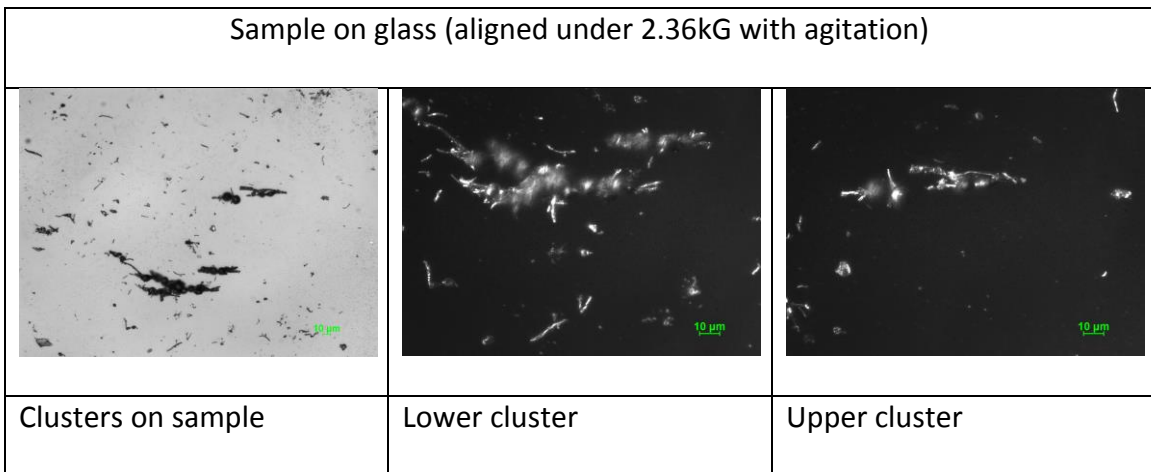


Figure 3.4 Sample on glass (aligned under 2.36kG after vortex agitation)

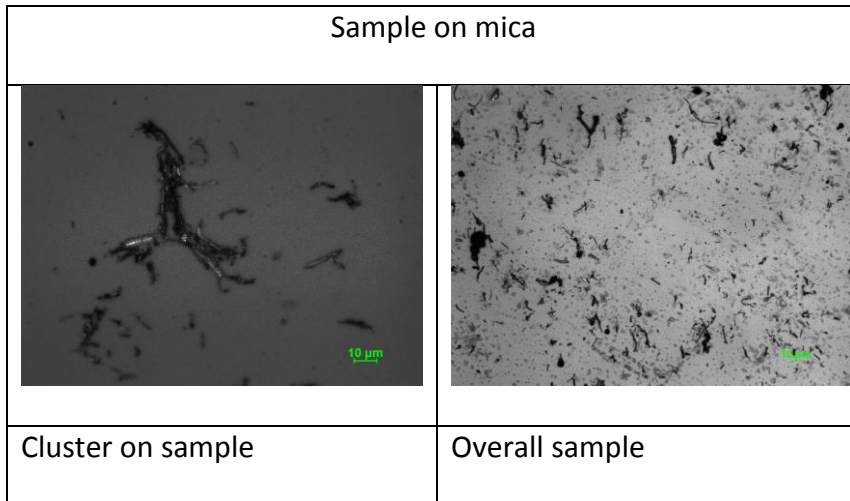


Figure 3.5 Sample on mica

From this alignment, three transmission experiment possibilities have been considered:

- SHG on a single nanofiber,
- SHG on a cluster,
- SHG on a group of nanofibers aligned in the same direction.

In principle, the best alignment will allow us to excite a group of fibers similarly oriented with the same incoming beam in order to increase the intensity of the generated SHG signal. This might be necessary because the SHG signal, which is already weak for the bulk barium titanate, is expected to be even weaker in our case, due to size effects (cf. analysis in the second chapter): the fibers are  $7\mu\text{m}$  long in average and their diameter is close to  $1\mu\text{m}$ . In addition, the CFO phase may increase the skin depth of these fibers. On the other hand, a cluster should also have a better response than a single fiber in term of intensity, but the light polarization dependence of the SHG signal should be different for the cluster, where the fibers are not “perfectly” aligned.



### 3. Sample holder and sample mount

The transmission sample holder has been prepared to fit the cryostation mount holder for vacuum and low temperature applications. It is made of oxygen free copper with two brass screws for the sample holder. It ensures a good thermal contact for round microscope glass cover slides of about 18 mm and prevents gas entrapment (fig. 3.6). The sample mount fits the sample holder: It is made of aluminum and can hold two different rubber silicon heaters for temperature dependent experiments. The two heaters A and B (fig 3.7) can be used together with the heater A in the center of the mount (fig. 3.10) or separately (fig. 3.8 and fig. 3.9) for different temperature ranges.

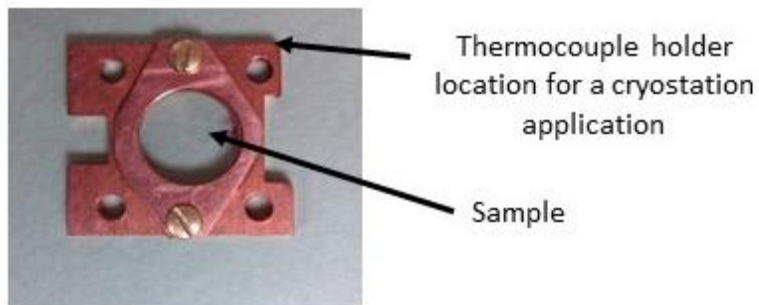


Figure 3.6 Sample holder



Figure 3.7 Heaters A and B



Figure 3.8 Heater A configuration (back side)

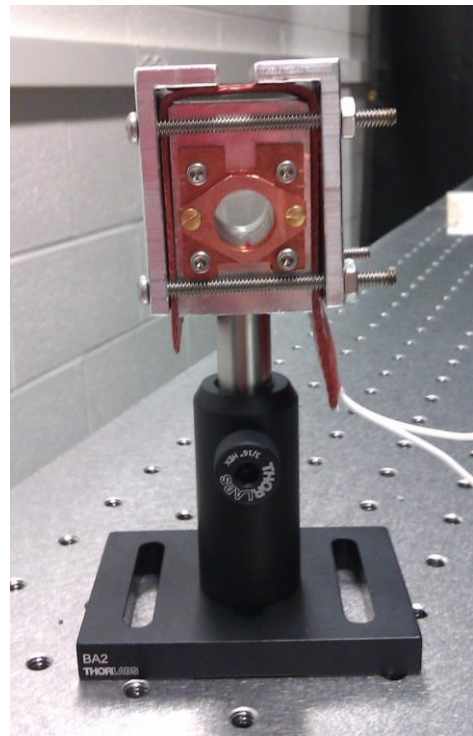


Figure 3.9 Heater B configuration (front side)

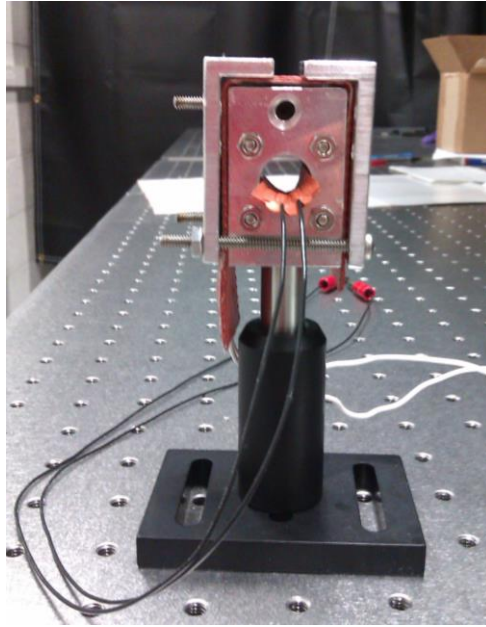


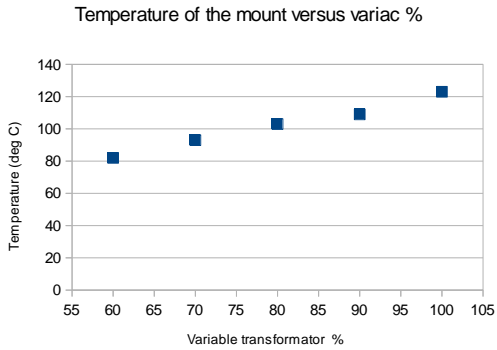
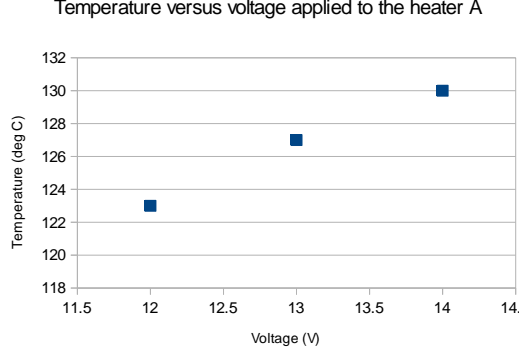
Figure 3.10 A + B configuration

Different calibrations have been done for the range of temperature of interest. The data for those calibrations are reported in the tables 3.1 and 3.2.

Table 3.1 Calibration: mount used with one heater alone

<p>Temperature of the mount versus Voltage applied Heater A alone</p> <table border="1"> <thead> <tr> <th>Voltage applied (V)</th> <th>Temperature (deg C)</th> </tr> </thead> <tbody> <tr> <td>9</td> <td>40</td> </tr> <tr> <td>10</td> <td>47</td> </tr> <tr> <td>11</td> <td>50</td> </tr> <tr> <td>12</td> <td>55</td> </tr> </tbody> </table>	Voltage applied (V)	Temperature (deg C)	9	40	10	47	11	50	12	55	<p>Temperature of the mount versus variable % Heater B alone (100% correspond to 120V)</p> <table border="1"> <thead> <tr> <th>Variable transformer %</th> <th>Temperature (deg C)</th> </tr> </thead> <tbody> <tr> <td>50</td> <td>40</td> </tr> <tr> <td>70</td> <td>62</td> </tr> <tr> <td>80</td> <td>70</td> </tr> <tr> <td>100</td> <td>95</td> </tr> </tbody> </table>	Variable transformer %	Temperature (deg C)	50	40	70	62	80	70	100	95
Voltage applied (V)	Temperature (deg C)																				
9	40																				
10	47																				
11	50																				
12	55																				
Variable transformer %	Temperature (deg C)																				
50	40																				
70	62																				
80	70																				
100	95																				
<p>Heater A configuration</p>	<p>Heater B configuration</p>																				

Table 3.2 Calibration: mount used with the two heaters together (A and B)

 <p>Temperature of the mount versus variac %</p>	 <p>Temperature versus voltage applied to the heater A</p>
<p>Voltage applied to the heater A = 12V DC</p>	<p>Voltage applied to the heater B = 120V AC  <i>Note: in this configuration, the voltage applied to the heater B exceed the maximum value suggested by the data sheet of the heater</i></p>

#### 4. Experiment alignment for SHG in transmission

As seen previously, the SHG signal is expected to be weak, especially due to size effects; as a consequence, the experiment requires a high intensity laser. We are using a Mira mode locked / pulsed with a frequency of 76 MHz at 840nm. The power is controlled by an upstream neutral density filter and a Glan-Taylor polarizer; the polarization angle of the incoming p-polarized light is controlled by a half-wave plate (cf. fig 3.11, where  $\lambda/2$  stands for half wave plate, PBS is a polarizer beam splitter, ND is a neutral density filter).

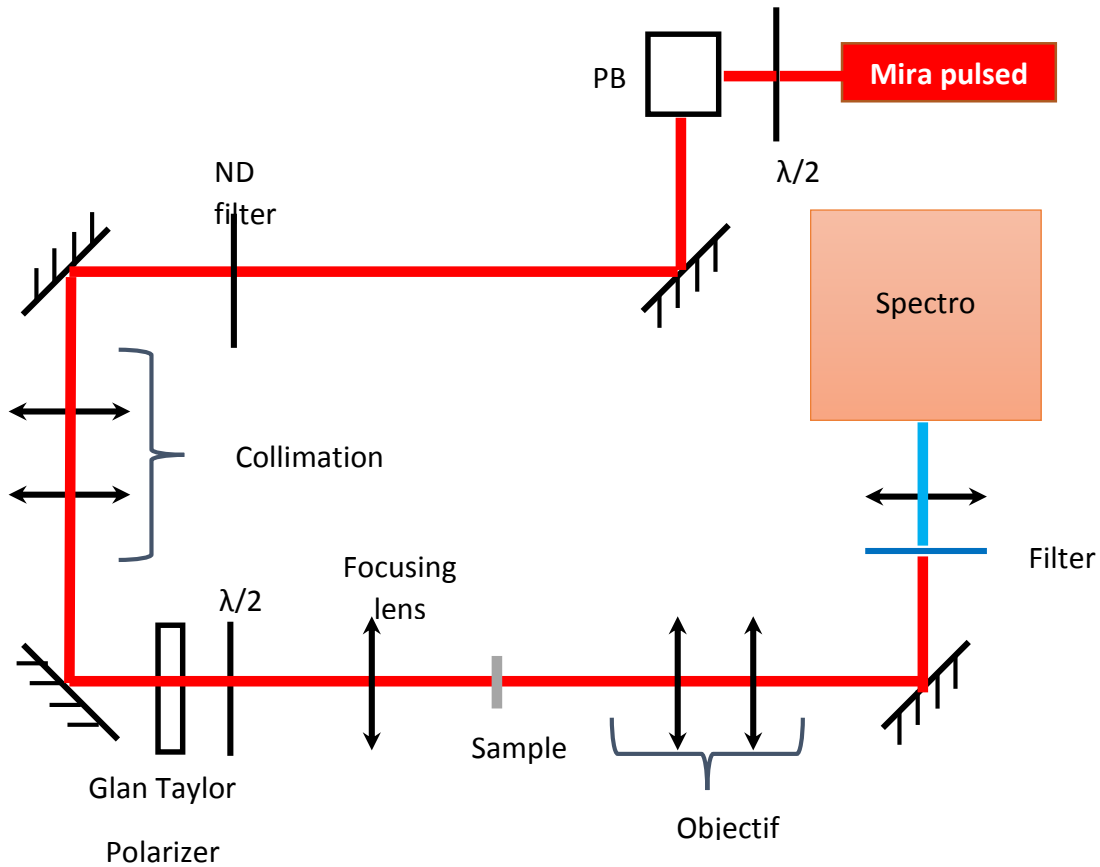


Figure 3.11 Experiment design

The focusing lens and the objective are mounted on a Z-stage and the sample is on a XYZ-stage. To clearly identify and pre-select the area of interest on the sample, a white source of light can be placed between the collimation and the Glan-Taylor polarizer, associated with a screen in front of the spectrometer. With a movable CCD camera located in the spectrometer, the sample area of interest may be refined, and it is possible to select a particular fiber or cluster. Again, the magnetic alignment of the fibers is convenient to choose a particular direction of the fiber with respect to the entry slit of the spectrometer. For now, only a short pass filter at 450 nm is used to block the excitation beam. It is epoxy

laminated and, in term of power, its best performance is about 1-10 J/cm<sup>2</sup>. An additional filter or a dichroic mirror may be used in the future.

## 5. Interdigital electrodes on glass

The electrodes have been prepared via photolithography (by projection) in the perspective of investigating the behavior of the fibers in an electric field. The exposure and development have been done following the procedure in Dr. Webb's lab. The projection of the interdigital electrodes pattern has been made using different line widths (the size has been adjusted via the "number of points" under power point), and the lines have been projected at the center of the image. We have measured the resulting lines just after the developing with an optical microscope (fig. 3.12, 3.13 and 3.14): the minimum width was found to be near the center of the pattern (probably due to distortions occurring near the edge of the whole projected image). A calibration has been done prior to the preparation of the pattern (fig. 3.15).

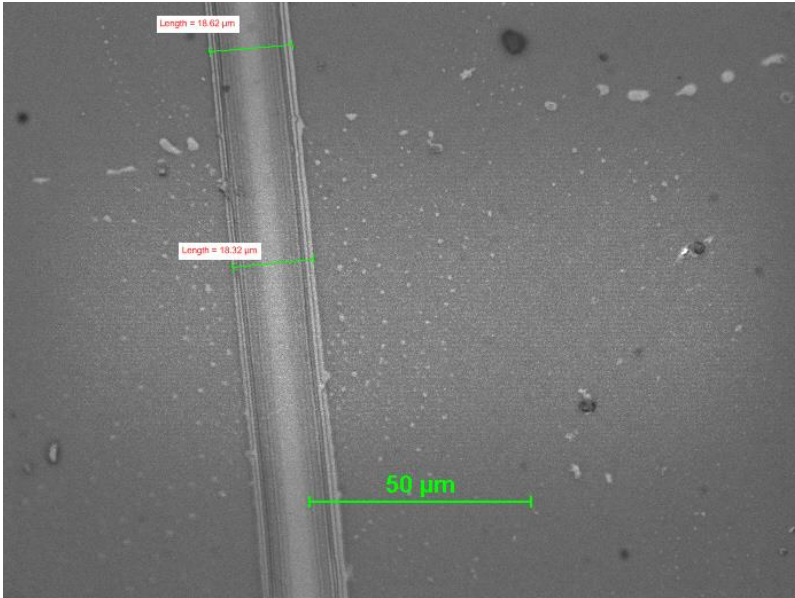


Figure 3.12 Measurements made for a line width of 20 points

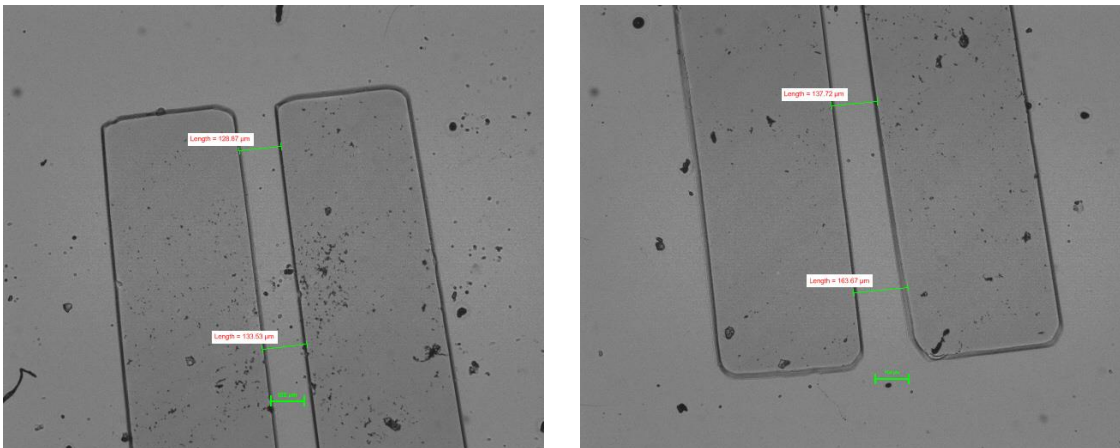


Figure 3.13 Measurements made for a line width of 50 points

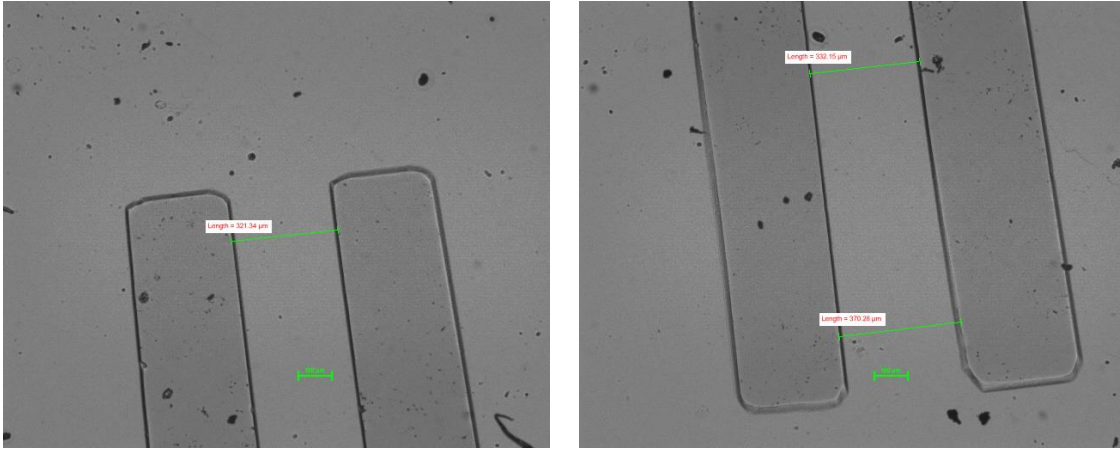


Figure 3.14 Measurements made for a line width of 100 points

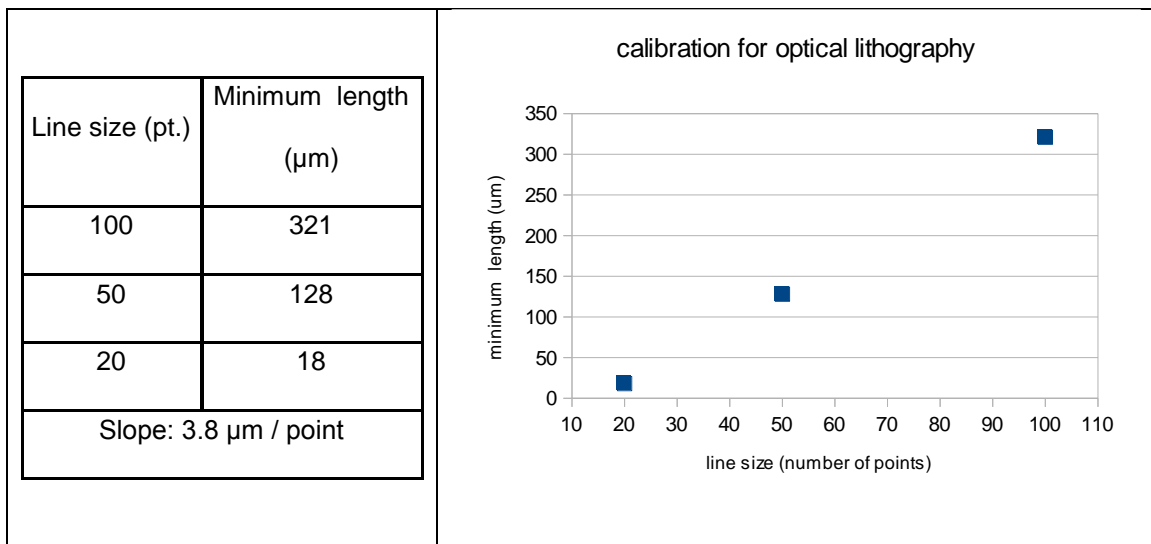


Figure 3.15 Calibration for the projection photolithography

In order to prepare fourteen samples during the same thermal evaporation, a sample holder has been prepared (fig 3.16), and the chromium and gold deposition has been made via thermal evaporation. We have prepared three types of electrodes (fig 3.17).





Figure 3.16 Sample holder

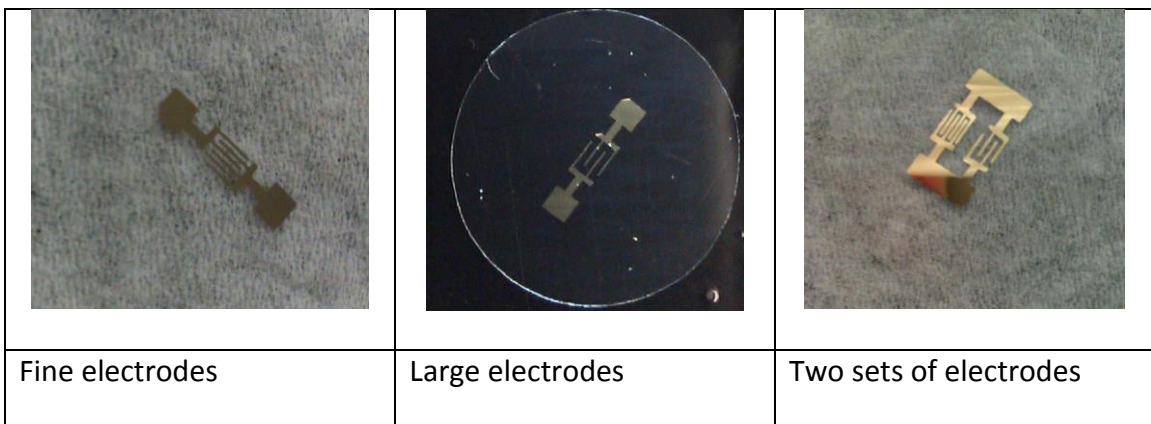


Figure 3.17 Interdigital electrodes

In principle, the different sets of electrodes should allow for different external electric field strengths.

## 6. Future plans: conduct of the experiment

We have discussed that the SHG signal is expected to monitor the Curie temperature of the ferroelectric phase. Also, the polarization dependence of the input laser should confirm the presence of the tetragonal phase as well as the angle between the  $a$  and  $c$

axis in the structure. We expect an eventual shift of the Curie temperature to a lower value compared to that of the bulk. This shift might reveal the importance of strain due to the CFO phase and other surface effects on the tetragonality. The alignment of the fibers is convenient as it allows for the excitation of a large group of nanofibers in order to increase the SHG signal, which might be weak for a single fiber due to possible absorption process and size effects. However, if the SHG signal from a single fiber is intense enough, we might consider investigating the influence of the fiber length on the previously discussed results (Curie temperature, presence of the tetragonal structure, polarization dependence). Finally, if the signal is too weak, it is still possible to prepare an experiment in reflection that might lower some absorption process.

We have also planned further experiments in an external electric field. It should confirm the presence of the tetragonal structure and emphasize any preferred direction for the generation of the SHG signal with respect to the main axis of the fibers. The different sets of electrodes allow for different maximum field strengths, depending on the distance between the interdigital electrodes. However, it is important to note that previous experiences conducted on barium titanate have required an electric field of about 2 MV/m in order to generate the hysteresis cycle for grain size ranging from 0.3  $\mu\text{m}$  to 1.2  $\mu\text{m}$ [16]. If no influence can be seen from the external electric field produced by our existing sets of electrodes, we plan to make electrodes with smaller separation distances via electron beam lithography in order to reach a higher field.

## Glossary

**Antiferroelectric:** material that possesses ordered dipole moment that can cancel each other in the unit cell.

**Antiferromagnetic:** material that possesses ordered magnetic moment that can cancel each other in the unit cell (in the localized sense).

**Diamagnetic:** exhibits a magnetization in response to an applied magnetic field, in the opposite direction than the applied field.

**Displacive phase transition:** transition with a single potential energy minimum whose position shifts at the transition temperature.

**Electrostriction:** change in strain as a quadratic function of an applied electric field.

**Ferrimagnetic:** material that possesses ordered magnetic moments that do not cancel each other completely, which results in a magnetization that can be switched in response to an applied magnetic field.

**Ferroelastic:** displays a spontaneous and stable deformation (phase change) that can be switched hysteretically by an applied stress.

**Ferromagnetic:** possesses a spontaneous magnetization that is stable and can be switched hysteretically by an applied magnetic field.

**Ferrotoroidic:** possesses a spontaneous and stable order parameter which is the curl of a polarization or magnetization.

**First order phase transition:** following the Ehrenfest classification, a first order transition has its first derivative of the free energy with respect to the order parameter discontinuous at the transition. (The order parameter associated with ferroelectricity is the polarization).

**Flexoelectric:** exhibits a spontaneous electrical polarization in response to a strain gradient.

**Magnetostriction:** change in strain as a quadratic function of an applied magnetic field.

**Order disorder phase transition:** transition with several minima among which a “choice” is made.

**Paramagnetic:** exhibits a magnetization in response to an applied magnetic field, in the same direction than the applied field (but does not have a spontaneous magnetization).

**Piezoelectric:** exhibits the generation of electrical charge in response to an applied mechanical stress, and vice-versa. The response is linear.

**Piezomagnetic:** exhibits a change of magnetization in response to an applied mechanical stress, and vice-versa. The response is linear.

**Pyroelectric:** has a spontaneous electric polarization that varies with the temperature.

**Second order phase transition:** following the Ehrenfest classification, a first order transition has its first derivative of the free energy with respect to the order parameter

continuous and its second derivative of the free energy with respect to the order parameter discontinuous at the transition.

## References

- [1] W. Eerenstein, N. D. Mathur, and J. F. Scott, "Multiferroic and magnetoelectric materials.," *Nature*, vol. 442, no. 7104, pp. 759–65, 2006.
- [2] Z. Surowiak and D. Bochenek, "Multiferroic materials for sensors, transducers and memory devices," *Arch. Acoust.*, vol. 33, no. 2, pp. 243–260, 2008.
- [3] A. Kargol, L. Malkinski, and G. Caruntu, "Biomedical Applications of Multiferroic Nanoparticles," *Adv. Magn. Mater.*, pp. 89–118, 2012.
- [4] S. L. Hou and N. Bloembergen, "Paramagnetoelectric Effects in  $\text{NiS O}_4 \cdot 6 \text{H}_2 \text{O}$ ," *Phys. Rev.*, vol. 138, no. 4A, pp. A1218–A1226, May 1965.
- [5] J. Varignon, D. Fontaine, E. Bousquet, N. C. Bristowe, and P. Ghosez, "Ferromagnetism induced by entangled charge and orbital orderings in ferroelectric titanate perovskites," *Nat. Commun.*, vol. 6, pp. 1–6, 2015.
- [6] P. Toladeno and V. Dmitriev, *Reconstructive phase transition: in crystal and quasicrystal*. 1996.
- [7] W. Zhong, D. Vanderbilt, and K. Rabe, "Phase Transitions in  $\text{BaTiO}_3$  from First Principles," *Phys. Rev. B*, vol. 73, no. 13, p. 1861, 1994.
- [8] J. Yu and J. Chu, "Nanocrystalline Barium Titanate," *Encycl. Nanosci. Nanotechnol.*, vol. 6, pp. 389–416, 2004.
- [9] T. P. Dougherty, G. P. Wiederrecht, K. a. Nelson, M. H. Garrett, H. P. Jenssen, and C. Warde, "Femtosecond time-resolved spectroscopy of soft modes in structural phase transitions of perovskites," *Phys. Rev. B*, vol. 50, no. 13, pp. 8996–9019, 1994.
- [10] K. Uchino, E. Sadanaga, and T. Hirose, "Dependence of the Crystal Structure on Particle Size in Barium Titanate," *J. Am. Ceram. Soc.*, vol. 72, no. 8, pp. 1555–1558, Aug. 1989.
- [11] M. Frey and D. Payne, "Grain-size effect on structure and phase transformations for barium titanate," *Phys. Rev. B*, vol. 54, no. 5, pp. 3158–3168, 1996.

- [12] H.-I. Hsiang and F.-S. Yen, "Effect of Crystallite Size on the Ferroelectric Domain Growth of Ultrafine BaTiO<sub>3</sub> Powders," *Journal of the American Ceramic Society*, vol. 79, pp. 1053–1060, 1996.
- [13] S. Schlag and H.-F. Eicke, "Size driven phase transition in nanocrystalline BaTiO<sub>3</sub>," *Solid State Commun.*, vol. 91, no. 11, pp. 883–887, Sep. 1994.
- [14] B. Bihari, J. Kumar, G. T. Stauf, P. C. Van Buskirk, and C. S. Hwang, "Investigation of barium titanate thin films on MgO substrates by second-harmonic generation," *J. Appl. Phys.*, vol. 76, no. 2, p. 1169, 1994.
- [15] D. Szwarcman, D. Vestler, and G. Markovich, "The size-dependent ferroelectric phase transition in BaTiO<sub>3</sub> nanocrystals probed by surface plasmons.," *ACS Nano*, vol. 5, no. 1, pp. 507–15, 2011.
- [16] T. Takeuchi, C. Capiglia, N. Balakrishnan, Y. Takeda, and H. Kageyama, "Preparation of Fine-grained BaTiO<sub>3</sub> Ceramics by Spark Plasma Sintering," *J. Mater. Res.*, vol. 17, no. 03, pp. 575–581, 2011.
- [17] S. Nambu and D. A. Sagala, "Domain formation and elastic long-range interaction in ferroelectric perovskites," *Phys. Rev. B*, vol. 50, no. 9, pp. 5838–5847, Sep. 1994.
- [18] A. Yariv, *Introduction to Optical electronics*. 1976.
- [19] R. C. Miller, "OPTICAL SECOND HARMONIC GENERATION IN PIEZOELECTRIC CRYSTALS," *Appl. Phys. Lett.*, vol. 5, no. 1, p. 17, 1964.
- [20] R. C. Eckardt and R. L. Byer, "Measurement of nonlinear optical coefficients by phase-matched harmonic generation," *Spie*, vol. 1561, pp. 119–127, 1991.
- [21] E. Kim, A. Steinbrück, M. T. Buscaglia, V. Buscaglia, T. Pertsch, and R. Grange, "Second-Harmonic Generation of Single BaTiO<sub>3</sub> Nanoparticles down to 22 nm Diameter," *ACS Nano*, vol. 7, no. 6, pp. 5343–5349, 2013.